VEDEM+: Enhancing Engineering Assessment of Complex Stereotomic Structures via 3DEC-to-CAD Post-Processing Workflows

Lino Cusano[1(✉)] and Antonino Iannuzzo[2]

[1] University of Sannio, Benevento, Italy
l.cusano@studenti.unisannio.it
[2] Department of Engineering, University of Sannio, Piazza Roma, 28, 82100 Benevento, Italy
aniannuzzo@unisannio.it

Abstract. The use of Distinct Element Methods such as 3DEC by Itasca is now widespread, not only for geotechnical analyses of discontinuous materials but also, in the last two decades, for the study of masonry structures. In recent years, DEM-based approaches have been successfully applied to block-based assemblies, including historical constructions and newly designed structures assembled with dry joints. In this context, while distinct element software enables the simulation of complex mechanical scenarios, it still lacks features that facilitate rapid engineering assessment and interpretation of results. This paper presents VEDEM+ (*Visualisation Environment for Distinct Element Method*), a dedicated post-processing plugin for Rhinoceros 8 developed by the authors, which enables in-depth interpretation of 3DEC results within a CAD environment. A stereotomic flat vault with complex geometry is used as a reference structural system to demonstrate how the proposed workflow enables a rapid and effective engineering assessment of structural response, with particular attention to contact force visualisation, interface failure tracking, and gap/penetration mapping across incremental loading steps.

Keywords: 3DEC · Distinct element modelling · Masonry · Flat vault · Stereotomy · Non-convex blocks · Rigid blocks · Force path · VEDEM+

1 Introduction

The construction industry is one of the main causes of global resource consumption and CO_2 emissions. For decades, attention has been placed primarily on reducing operational energy, obtaining remarkable results, while embodied emissions now represent the central environmental challenge. To address this, the Reduce-Reuse-Recycle methodology provides a rigorous framework: reuse of

© The Author(s), under exclusive license to Springer Nature Switzerland AG 2027
O. Gervasi et al. (Eds.): ICCSA 2026 Workshops, LNCS 16758, pp. 564–580, 2027.
https://doi.org/10.1007/978-3-032-30497-1_34

structural components alone can reduce embodied carbon by 40–70% compared to recycling [7,16].

Floor systems are a primary target: in medium-to-high-rise buildings, floors account for over 40% of total structural mass and embodied emissions [6,58]. The widespread use of the reinforced concrete flat slab is both materially inefficient and incompatible with circularity, since the steel-concrete composite bond prevents component reuse or clean material recovery.

Compression-based structural systems offer an efficient alternative. Recently built examples confirm their viability: the *Striatus* footbridge and its second iteration *Phoenix* [4,17], developed at ETH Zurich, demonstrated that dry-assembled unreinforced concrete voussoirs can be fully disassembled and their material reused or recovered. Applied to floor systems, the Rippmann Floor System (RFS) [6,59] showed that compression-based funicular geometries can reduce concrete mass by 67–75% and reinforcement steel by approximately 90% compared to conventional reinforced concrete flat slabs of equivalent span. In this logic, the stereotomic flat vault system represents a historically grounded extension, combining compression-only load transfer with the inherent disassemblability of dry-assembled masonry, directly addressing circularity imperatives. Their structural behaviour, however, is considerably more complex than double-curved shells: large horizontal thrusts, sensitivity to joint geometry, and vulnerability to support displacements make numerical assessment essential [30,39,42,45]. Cracks can appear, drastically redirecting the internal flow of forces and significantly changing the thrusts exerted on the supports. However, since the seminal work of Heyman [26], it has been understood that cracks are not a structural concern [46], as arched structures can experience significant deformation until collapse, as demonstrated in experimental tests [15,20–22,25].

Several methods have been developed to assess the stability of masonry structures, using revised versions of graphic statics [12–14,49], rigid block approaches [23,24,27,44,57], continuous approaches [19,34,41], and finite element approaches based on limit analysis [8,55,56]. Flat vaults are particularly sensitive to support displacements, and several 2D and 3D models have been developed to investigate the mechanical response of masonry systems to boundary conditions [20,21,25,29,31–33]. Optimisation-based methods have also been developed to capture the 3D mechanical response in terms of internal forces, including discontinuous approaches such as Thrust Network Analysis [2,43] and continuous methods such as Membrane Equilibrium Analysis [1,40,47–49].

In general, masonry can be modelled using two main strategies [37,38]. Equivalent continuum (macro) models treat masonry as a homogeneous material with smeared properties, suitable for large-scale assessments but unable to capture local joint behaviour. Discontinuum (micro) models represent joints explicitly, as interface elements in the Finite Element Method (FEM) or contacts in the Distinct Element Method (DEM), providing accurate simulation of fracture, sliding, and opening at a higher computational cost. A numerical technique qualifies as a Distinct Element Method if it satisfies three assumptions [9]: (i) the model is composed of distinct finite elements that can be either rigid or deformable;

(ii) large displacements are permitted; (iii) contact topology is automatically tracked and updated, allowing the formation of new contacts between blocks. These features are well-suited for masonry structures, with nonlinearity concentrated in the contacts [3,37,38], and in particular for stereotomic flat vaults, whose structural behaviour is governed entirely by joint geometry and mechanics. Moreover, the limited number of blocks (order of tens) makes a full DEM micro-model computationally tractable [18].

The application of DEM to masonry structures has a well-established research lineage. Among the earliest contributions were nonlinear seismic analyses of drum columns at the Temple of Apollo at Bassae [52], subsequently validated against shaking table tests on a 1:3 marble model of a Parthenon column [51]. Masonry arches were an early focus of DEM studies: Pagnoni and Vanzi [50] and Lemos [36] investigated arch behaviour under various loading and support conditions. Subsequent work extended DEM to barrel vaults, groin vaults, and doubly-curved shells [18,39,53,54,61].

Several software environments implement the DEM for the analysis of masonry structures. 3DEC [35] is the three-dimensional extension of UDEC and is today one of the most widely used commercial platforms for structural masonry analysis. It models elements as convex polyhedra or assemblies of convex sub-blocks, treated as either rigid or deformable, with contacts automatically detected and discretised into sub-contacts at nodal intersection points. Discontinuous Deformation Analysis (DDA), introduced by [63], uses an implicit time integration strategy and models blocks with a uniform strain field, offering greater numerical stability at the cost of potential convergence difficulties in problems with frequently changing contact topologies.

This paper presents the potential offered by VEDEM+, an in-house developed plugin for Rhinoceros 8 that provides a dedicated post-processing environment for analyses carried out with 3DEC 9.0 by Itasca. The plugin addresses a series of practical limitations that users typically face when working in DEM software, particularly for the analysis of block-based structures with attention to early-stage design and engineering interpretation.

2 3DEC Software Features

As detailed above, in general, as other DEM solvers, 3DEC is selected as the modelling environment for three reasons: its three-dimensional formulation for capturing the structural response; the flexibility in assigning material properties to match the physical characteristics of real and 3D-printed specimens; and the ability to extract data and develop custom post-processing routines.

2.1 Block Modelling Options

3DEC offers three ways to model blocks based on how rigidity and internal deformation are handled.

Perfectly rigid blocks treat each block as a rigid body with six degrees of freedom. All forces are reduced to the centroid, generating resultant force and moment vectors; the equations of motion directly yield translational and rotational accelerations at each time step. This formulation requires minimal material property input, is computationally efficient, and is physically accurate whenever joint compliance vastly exceeds block compliance, as is the case for strong stone masonry or hard 3D-printed blocks.

Deformable blocks are modelled by subdividing each polyhedral block into an internal mesh of tetrahedral finite elements with uniform strain [11]. Nodal translations are the kinematic unknowns; the equations of motion are applied to nodal accelerations, allowing evaluation of internal stress distributions. For most masonry analyses, deformable blocks are treated as elastic, since nonlinear behaviour is primarily associated with joint interactions; however, elasto-plastic or damage constitutive laws can also be assigned, and user-defined models are supported through FISH.

Joined block groups are generated by merging adjacent blocks into a single kinematic unit via the `block join` command [35]. The interface between joined blocks permits no relative displacement, slip, or separation, and generates no force contribution to the equations of motion. Joining is the primary mechanism for creating non-convex geometries in 3DEC: a non-convex voussoir is decomposed into convex sub-blocks, which are then joined to behave as a single unit (Fig. 4). In the present study, deformable blocks are modelled without internal plasticity; structural nonlinearity is therefore exclusively concentrated at the un-joined dry joints.

2.2 Contact Representation and Constitutive Models

In 3DEC, contacts are modelled using the point contact approach [37], with the common plane concept used to handle contact detection efficiently [10]. Once two blocks are identified as being in contact, 3DEC defines specific sub-contacts based on the geometry of the interaction. The mechanical behaviour at each sub-contact is governed by a joint constitutive model; the most widely adopted is the Mohr-Coulomb model with tension cut-off, requiring normal stiffness k_n, shear stiffness k_s, friction angle, cohesion, and tensile strength as input parameters. Contact stiffness is a critical parameter: an excessively low normal stiffness leads to unrealistic block interpenetration, governed by:

$$\Delta\sigma_n = k_n \, \Delta u_n \tag{1}$$

3 VEDEM+: a 3DEC-to-CAD Post-Processing Plugin

Despite the widespread use of DEM tools, a practical gap remains between numerical analysis and the engineering interpretation of results. A typical displacement capacity analysis involves a sequence of tens to hundreds of incremental steps, each producing outputs such as block positions, velocities, and interface forces. Assembling these data into readable force paths, force-displacement

curves, and joint-level Mohr-Coulomb failure checks, as well as visualising deformed geometries and comparing results across loading steps, requires significant manual effort that is difficult to automate within the 3DEC scripting environment alone. Moreover, the built-in visualisation tools of 3DEC offer limited parametric flexibility compared to dedicated CAD environments such as Blender [5] or Rhino [60], where extensive Python libraries are readily available.

3.1 Architecture and Data Exchange

VEDEM+ is written in C# targeting the .NET 7.0 runtime, the standard managed environment for Rhino 8 on Windows, using the RhinoCommon SDK and the Eto.Forms a cross-platform UI framework. The choice of a compiled language over Python-based scripting was deliberate: parsing large JSON files encoding the full block geometry, displacement, and contact state of models with dozens of blocks and hundreds of sub-contacts requires the performance and type safety of C#.

Communication between 3DEC and the plugin is mediated by JSON files generated at the end of each loading step by FISH scripts executed within the solver. Three categories of files are produced per step:

- **Block export**: vertex coordinates and face connectivity in the deformed configuration, together with centroid scalar quantities (displacement, velocity, applied and unbalanced forces, mass, volume).
- **Subcontact export**: for each contact pair, the list of active sub-contacts with position, area, normal and shear forces, normal and shear displacements, slip state, and gap value.
- **Penetration export**: normal gap at each sub-contact, enriched with the contact normal vector and tributary area, used to drive the oriented-disc visualisation described below.

This three-tier structure separates block-level quantities, contact-level state, and gap/penetration data, each loaded independently by the plugin. All imported steps are organised under a named layer hierarchy in Rhino (`3DEC::step_N`), enabling direct visual comparison between steps by toggling layer visibility.



Fig. 1. VEDEM+ pipeline: from CAD geometry definition to 3DEC analysis and back to the CAD environment for post-processing and visualisation.

3.2 Modelling Workflow

The computational pipeline used to model and analyse the flat vault consists of three stages, summarised in Fig. 1. The vault geometry is defined parametrically in a CAD environment, modelling voussoirs, supporting abutments, and connection elements. Non-convex voussoirs are decomposed into convex sub-blocks for compatibility with 3DEC's contact detection (Fig. 4); once imported, sub-blocks are rejoined via the `block join` command to reconstruct the original non-convex shapes (Fig. 3a). Analyses are performed directly in 3DEC, including incremental displacement capacity, load-bearing or dynamic tests (Fig. 3b). This sequence of results is then exported back to Rhino, where VEDEM+ is used to visualise and interpret the structural response (Fig. 5).

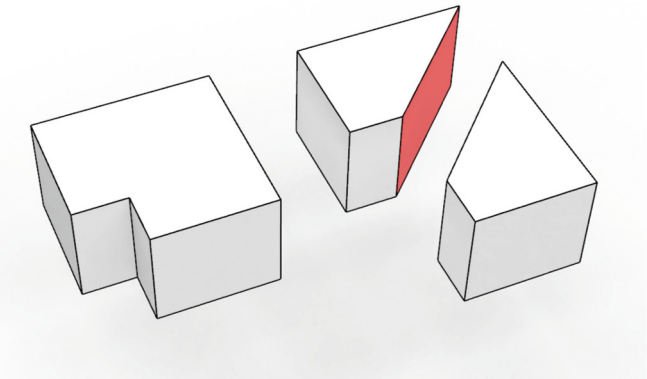

Fig. 2. A non-convex block reconstructed by joining two convex sub-blocks. When blocks are modelled as rigid, the red interface is locked and no forces can be derived from the 3DEC calculation. (Color figure online)

3.3 Visualisation Features

VEDEM+ provides four main visualisation modules, each addressing a specific analytical need.

Block Scalar Heatmaps. Each block is rendered as a triangulated mesh and coloured according to any scalar field available in the data model: displacement components and magnitude, velocity, unbalanced force, applied force, mass, or volume. A sequential five-stop palette (blue to red) is applied, normalised to the observed range within the current step, with min/max values displayed in the legend panel (Fig. 3b).

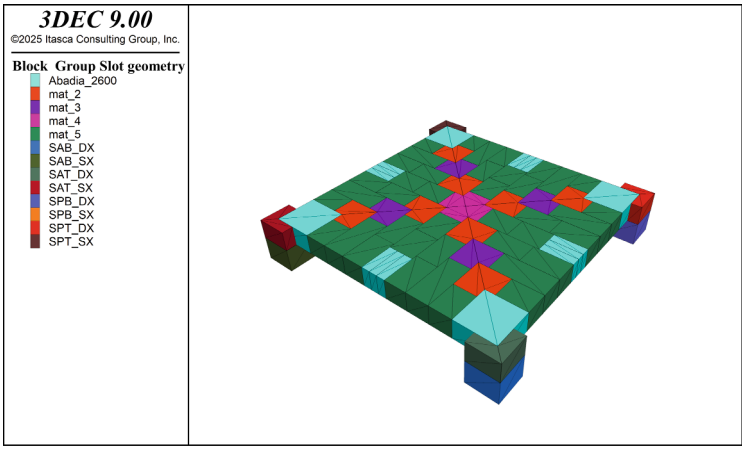

(a)

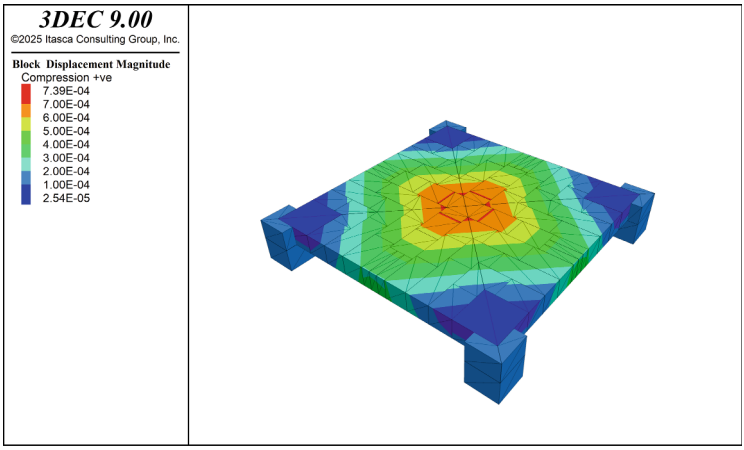

(b)

Fig. 3. (a) Non-convex block geometry reconstructed in 3DEC by joining convex sub-blocks via the `block join` command, with each block family identified by a distinct colour; (b) typical 3DEC displacement heatmap at a given loading step: while the solver output is complete, extracting engineering-relevant quantities requires significant additional effort.

Contact and Subcontact Force Visualisation. At the contact level, the plugin draws the resultant normal force N, tangential force T, and total resultant R as scaled line segments anchored at the centre of pressure of each interface. The sign convention follows 3DEC's native convention: positive normal force indicates compression. Normal components are shown in blue, tangential components in red, providing an immediate visual assessment of load paths through the joint

network (Fig. 5). At the subcontact level, forces are rendered as coloured spheres or oriented flat discs, with colour encoding the chosen scalar quantity through the same sequential heatmap.

Gap and Penetration Mapping. For each sub-contact, the normal gap g is defined as:

$$g = a_{\text{ini}} + u_n \tag{2}$$

where a_{ini} is the initial mechanical aperture and u_n is the accumulated normal displacement (positive in tension). A negative gap indicates interpenetration (closed, loaded contact); a positive gap indicates joint opening. Each sub-contact is rendered as a flat circular disc oriented with its axis parallel to the contact normal, with radius computed as $r = \sqrt{A_{\text{sc}}/\pi}$, ensuring that adjacent discs tessellate the joint surface without overlap. A divergent colour scheme encodes the gap value: penetrating contacts use a blue-to-red heatmap; opening contacts are rendered in blue tones (Fig. 7). This visualisation proved particularly effective for tracking the progressive detachment of joint faces as support displacement was incremented.

Interface Force History and Mohr-Coulomb Tracking. The Interfaces tab constitutes the primary analytical module for investigating per-contact force histories across the loading sequence. Interactive handles, represented by polygon hulls projected onto each contact plane, are generated at the centre of pressure of each

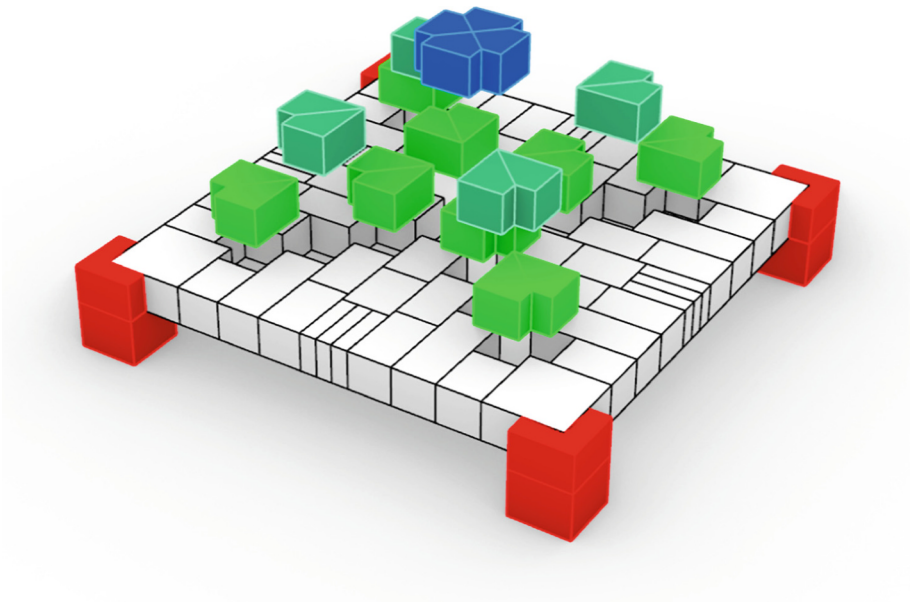

Fig. 4. A 3D view of the four non-convex block families, each identified by a distinct colour.

interface. Selecting a handle opens an Interface detail dialog displaying real-time metrics for the active step: resultant forces ($|N|$, $|T|$, $|R|$), the T/N ratio, torque, and the centre of pressure coordinates.

The Charts tab provides four synchronised plots visualising the evolution of N, T, R, and the T/N friction ratio across all loaded steps (Fig. 6). The friction ratio chart includes a dashed red line representing the Mohr-Coulomb failure threshold $\tan\phi$, where ϕ is automatically extracted from the sub-contact data but can be manually overridden to trigger an immediate re-rendering. An interactive crosshair tooltip snaps to the nearest data point and displays exact values at each step, removing the need to export data to a spreadsheet for inspection. A batch export function iterates automatically over every contact in the model, producing four PNG charts and one structured CSV file per interface, eliminating the need to open each dialog individually.

4 Application to the Flat Vault

The flat vault used as a structural case study to demonstrate the capabilities of VEDEM+ is a simplified digital model (Fig. 4) of a real structure built in Spain by the construction company Mass Piedra [62] and designed by Prof. Enrique Rabasa of the Politecnica de Madrid. As part of an ongoing collaboration, the research group at the University of Sannio was invited to assess the structural response of the vault in situ. A dedicated paper presenting the full-scale analysis on the real model and structural behaviour is forthcoming. In the present work, the geometry serves exclusively as a reference application to demonstrate how VEDEM+ can provide engineering-relevant insight in a real-case scenario. The

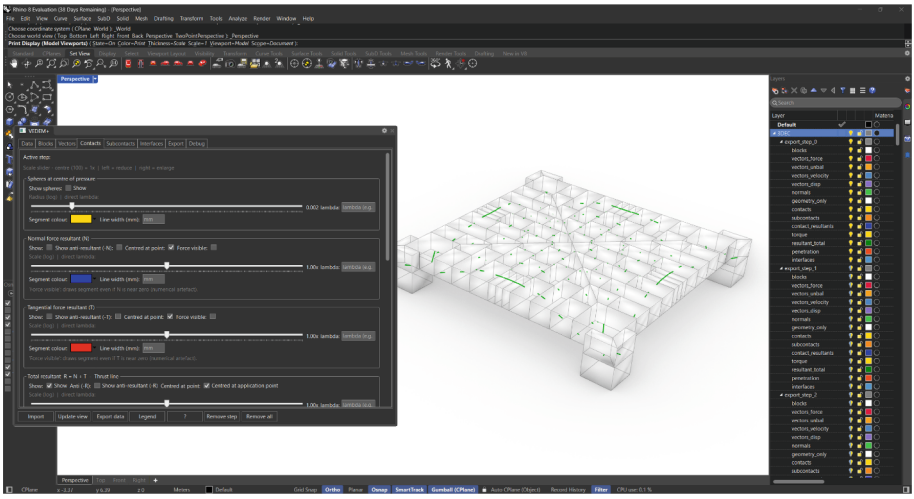

Fig. 5. VEDEM+ visualisation of contact interface resultant forces: arching behaviour visible from top and lateral views, unavailable in the native 3DEC environment.

four families of non-convex blocks are identified by distinct colours in Fig. 4; the model is imported into 3DEC, where dedicated scripts automatically join the convex sub-blocks and set up the analysis (Fig. 3).

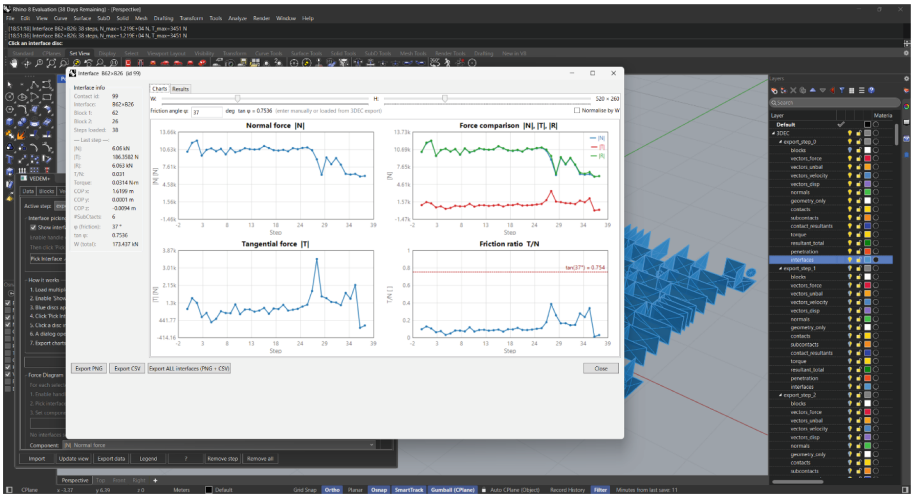

Fig. 6. VEDEM+ interface force history for a user-selected contact: evolution of N, T, R, and T/N across loading steps, with the Mohr-Coulomb threshold ($\tan\phi$) shown as a dashed red line. (Color figure online)

Four structural characteristics make the DEM analysis of flat vaults more demanding than other standard masonry typologies and motivate the use of a dedicated post-processing workflow.

Sensitivity to Joint Geometry: the stereotomy is designed to activate internal force paths orthogonal to the joints. Small deviations from the designed geometry, due to fabrication tolerances or assembly imperfections, can significantly alter the internal force distribution and structural stability [26,28].

Large Horizontal Thrusts: flat vaults generate very large horizontal thrusts relative to their vertical load-carrying capacity. The thrust-to-weight ratio is substantially higher than that of a typical semicircular arch of the same span, making stability highly sensitive to the stiffness and displacement of the lateral supports.

Coupled Sliding and Hinging Mechanisms: flat vault collapse typically involves a combination of sliding and hinging at block interfaces. The relative contribution of each mechanism depends on the joint friction angle and contact stiffnesses.

Sensitivity to Support Displacements: even small outward movements of the abutments can trigger collapse, requiring careful tracking of interface force evolution throughout the loading sequence.

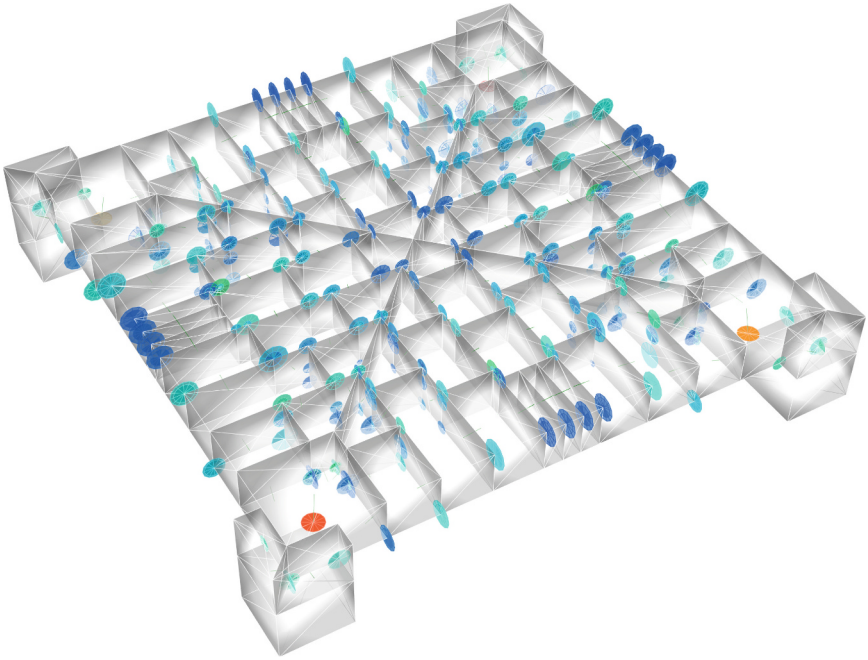

Fig. 7. VEDEM+ gap and penetration mapping: oriented discs are placed at subcontact positions where block interpenetration exceeds a user-defined threshold, encoding contact force magnitude via a blue-to-red colour scale, with warmer tones indicating higher compressive forces; joint opening is identified on the opposite face regions. (Color figure online)

VEDEM+ was used systematically throughout the analysis. The block geometry export allowed the deformed shape of the assembly to be visualised at each settlement increment alongside the original CAD model, providing an intuitive check of physical consistency. The subcontact force visualisation was used to track the evolution of the internal force distribution as support displacement was incremented; the normal force heatmap on joint faces provided a spatial reading of compression trajectories, whose progressive concentration at the extrados and intrados of selected joints is the signature of hinge formation Fig. 8. The gap and penetration maps were instrumental in identifying the sequence of joint openings, allowing the redistribution of internal forces to be followed step by step and correlated with the displacement histories exported by 3DEC (Fig. 7). The interface force history charts enabled direct verification of whether the T/N ratio at each joint remained within the Mohr-Coulomb cone throughout the loading sequence, providing a rigorous, step-resolved picture of the sliding-to-hinging transition.

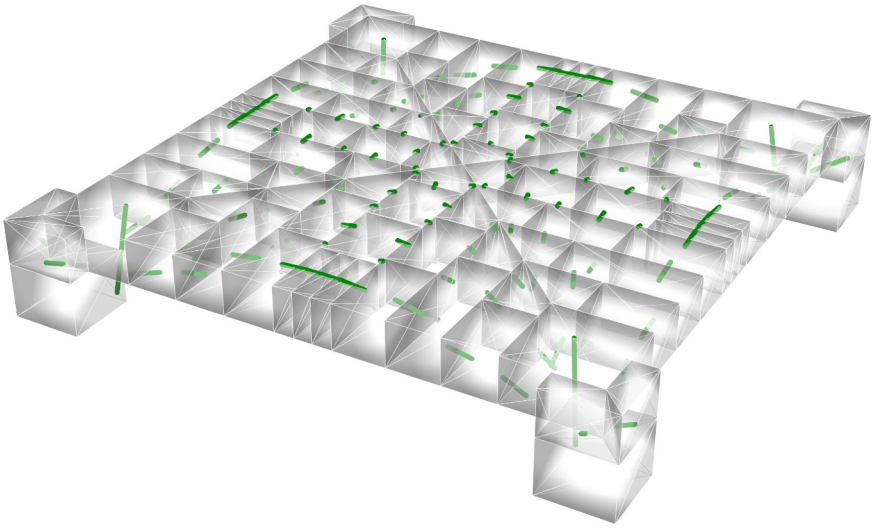

Fig. 8. VEDEM+ visualisation of contact resultant forces across the flat vault assembly.

5 Conclusions

This paper has presented VEDEM+, a post-processing plugin for Rhinoceros 8 developed to bridge the output of the 3DEC solver with a fully controllable CAD environment. The plugin addresses a practical gap in existing DEM workflows: while 3DEC is a mature and capable solver, its native visualisation tools are not well suited to the engineering interpretation of incremental analyses of block-based masonry structures. The plugin provides four main capabilities: block scalar heatmaps for deformed geometry inspection; contact and subcontact force visualisation with resultant diagrams; gap and penetration mapping via oriented discs; and per-interface force history tracking with integrated Mohr-Coulomb failure assessment. Applied to the analysis of a stereotomic flat vault, VEDEM+ enabled a step-resolved interpretation of the sliding-to-hinging transition, the progressive formation of hinges, and the redistribution of internal forces in response to support displacement. Current limitations include the absence of zone-level stress visualisation for deformable blocks, per-step colour normalisation rather than global normalisation across the loading sequence, and a file-based data exchange that introduces overhead for large models. Future developments will address these limitations through zone data export, global heatmap normalisation, and a live connection between 3DEC and Rhino via a shared memory buffer or local socket. A further planned development is a standalone viewer, independent of any specific CAD environment, allowing engineers to inspect and interrogate DEM results.

Acknowledgments. The authors warmly thank Prof. Enrique Rabasa and Catalina Sànchez Robles of Mass Piedra for generously sharing the geometry of the flat vault and for their kind collaboration. The real-scale experience on the vault at Caravaca de la Cruz, Spain, motivated the intensive development of VEDEM+ as a tool for detailed engineering assessment of structural response; both the features implemented and those planned for future releases were directly inspired by the practical needs encountered during that experience, which was therefore adopted as the reference case study given its geometric complexity. This research is funded by the Italian Ministry of University and Research through the Programme "Rita Levi Montalcini for Young Researchers" (FFO 2020). The authors gratefully acknowledge Itasca for providing the 3DEC software under the Educational Discount Agreement.

References

1. Angelillo, M., Iannuzzo, A., Montanino, A.: Discretised continuum approaches: from continuum to dis-continuum. In: Discrete Computational Mechanics of Masonry Structures, pp. 95–163. Springer (2023). https://doi.org/10.1007/978-3-031-32476-5_3
2. Avelino, R.M., Iannuzzo, A., Van Mele, T., Block, P.: Assessing the safety of vaulted masonry structures using thrust network analysis. Comput. Struct. **257**, 106647 (2021). https://doi.org/10.1016/j.compstruc.2021.106647
3. Bagi, K., Angelillo, M.: Discrete Computational Mechanics of Masonry Structures, vol. 609. Springer Nature (2023). https://doi.org/10.1007/978-3-031-32476-5
4. Bhooshan, S., Dell'Endice, A., Ranaudo, F., Van Mele, T., Block, P.: Unreinforced concrete masonry for circular construction. Architectural Intelligence **3**(1), 7 (2024). https://doi.org/10.1007/s44223-023-00043-y
5. Blender Foundation: Blender - a 3D modelling and rendering package. Blender Foundation, Amsterdam (2024). http://www.blender.org
6. Block, P.: Strength through geometry and material effectivenes, pp. 72–78. (2022). no open-access link available
7. Brütting, J., De Wolf, C., Fivet, C.: The reuse of load-bearing components. In: IOP Conference Series: Earth and Environmental Science. vol. 323, p. 012025 (2019). https://doi.org/10.1088/1755-1315/323/1/012025,
8. Buzzetti, M., Pingaro, N., Milani, G.: Automatic detection of local collapse mechanisms in historical masonry buildings: Fast and robust fe upper bound limit analysis. Eng. Fail. Anal. **170**, 109310 (2025). https://doi.org/10.1016/j.engfailanal.2025.109310
9. Cundall, P.A.: A computer model for simulating progressive, large-scale movements in blocky rock systems. In: Proceedings of the Symposium of the International Society of Rock Mechanics. vol. 1, pp. II–8. Nancy, France (1971). https://www.researchgate.net/publication/285299738
10. Cundall, P.A.: Formulation of a three-dimensional distinct element model – Part I: A scheme to detect and represent contacts in a system composed of many polyhedral blocks. Int. J. Rock Mech. Mining Sci. Geomech. Abstracts **25**(3), 107–116 (1988). https://doi.org/10.1016/0148-9062(88)92293-0
11. Cundall, P.A., Strack, O.: A discrete numerical model for granular assemblies. Géotechnique **29**(1), 47–65 (1979). https://doi.org/10.1680/geot.1979.29.1.47

12. Cusano, C., Angjeliu, G., Montanino, A., Zuccaro, G., Cennamo, C.: Considerations about the static response of masonry domes: A comparison between limit analysis and finite element method. Int. J. Masonry Res. Innov **6**(4), 502–528 (2021). https://doi.org/10.1504/IJMRI.2021.118835
13. Cusano, C., Montanino, A., Cennamo, C., Zuccaro, G., Angelillo, M.: Geometry and stability of a double-shell dome in four building phases: the case study of Santa Maria Alla Sanità in Naples. Int. J. Architectural Heritage **17**(2), 362–388 (2023). https://doi.org/10.1080/15583058.2021.1922954
14. Cusano, C., Montanino, A., Olivieri, C., Paris, V., Cennamo, C.: Graphical and analytical quantitative comparison in the Domes assessment: The case of San Francesco di Paola. Appl. Sci. **11**(8), 3622 (2021). https://doi.org/10.3390/app11083622
15. Daponte, P., De Vito, L., Iannuzzo, A., Monaco, M., Neyestani, A., Picariello, F.: Low-cost marked tracking monitoring system for 3D-scaled masonry models. In: 2024 IEEE International Workshop on Metrology for Living Environment (MetroLivEnv), pp. 172–177. IEEE (2024). https://doi.org/10.1109/MetroLivEnv60384.2024.10615826
16. De Wolf, C., Hoxha, E., Fivet, C.: Comparison of environmental assessment methods when reusing building components: A case study. Sustain. Cities Soc. **61**, 102322 (2020). https://doi.org/10.1016/j.scs.2020.102322
17. Dell'Endice, A., Bouten, S., Van Mele, T., Block, P.: Structural design and engineering of striatus, an unreinforced 3d-concrete-printed masonry arch bridge. Eng. Struct. **292**, 116534 (2023). https://doi.org/10.1016/j.engstruct.2023.116534
18. Dell'Endice, A., Iannuzzo, A., DeJong, M.J., Van Mele, T., Block, P.: Modelling imperfections in unreinforced masonry structures: Discrete element simulations and scale model experiments of a pavilion vault. Eng. Struct. **228**, 111499 (2021). https://doi.org/10.1016/j.engstruct.2020.111499
19. Fortunato, A., Gesualdo, A., Mascolo, I., Monaco, M.: P-Bézier energy optimisation for elastic solutions of masonry-like panels. Int. J. Masonry Res. Innov. **7**(1–2), 113–125 (2022). https://doi.org/10.1504/IJMRI.2022.119857
20. Galassi, S.: An alternative approach for limit analysis of masonry arches on moving supports in finite small displacements. Eng. Fail. Anal. **145**, 107004 (2023). https://doi.org/10.1016/j.engfailanal.2022.107004
21. Galassi, S., Misseri, G., Rovero, L.: Capacity assessment of masonry arches on moving supports in large displacements: Numerical model and experimental validation. Eng. Fail. Anal. **129**, 105700 (2021). https://doi.org/10.1016/j.engfailanal.2021.105700
22. Galassi, S., Misseri, G., Rovero, L., Tempesta, G.: Failure modes prediction of masonry voussoir arches on moving supports. Eng. Struct. **173**, 706–717 (2018). https://doi.org/10.1016/j.engstruct.2018.07.015
23. Galassi, S., et al.: A numerical tool for assessing the effect of foundation settlements on the stability of masonry walls. In: International Conference of Architecture, Engineering, and Design for Monuments Safeguarding, pp. 498–509. Springer (2025). https://doi.org/10.1007/978-3-032-15387-6_34
24. Galassi, S., Tempesta, G.: Safety assessment of masonry undamaged and damaged arches subjected to gravitational loads and horizontal forces. a numeric procedure to identify the optimal thrust line. Int. J. Solids Struct. **301**, 112943 (2024). https://doi.org/10.1016/j.ijsolstr.2024.112943
25. Galassi, S., Zampieri, P.: A new automatic procedure for nonlinear analysis of masonry arches subjected to large support movements. Eng. Struct. **276**, 115359 (2023). https://doi.org/10.1016/j.engstruct.2022.115359

26. Heyman, J.: The stone skeleton. Int. J. Solids Struct. **2**(2), 249–279 (1966). https://doi.org/10.1016/0020-7683(66)90018-7
27. Hua, Y., Buzzetti, M., Pingaro, N., da Silva, L.C., Milani, G.: A computerized tool for the kinematic limit analysis of 2d masonry structures failing on a tilting table. SoftwareX **30**, 102180 (2025). https://doi.org/10.1016/j.softx.2025.102180
28. Huerta, S.: Wedges and Plate Bandes Mechanical Theories After De La Hire En L Architrave Le Plancher La Plate Forme Nouvelle Histoire De La Construction Pag 405 435 Presses Polytechniques Et Universitaires Romandes (2012). Wedges and plate-bandes: mechanical theories after de la hire
29. Iannuzzo, A., Musone, V., Ruocco, E.: A neural network-based automated methodology to identify the crack causes in masonry structures. Comput.-Aided Civil Infrastructure Eng. **39**(24), 3769–3785 (2024). https://doi.org/10.1111/mice.13311
30. Iannuzzo, A., Bagi, K., Herczeg, M., Mousavian, E.: Equilibrium analysis of 2d complex discrete assemblies modelled using cracking blocks with non-dilatant interfaces. In: Proceedings of the Fifteenth International Conference on Computational Structures Technology, pp. 1–14. Civil-Comp Press (2024)
31. Iannuzzo, A., Gesualdo, A., Olivieri, C., Montanino, A.: 3d exploration of internal stresses due to lateral loads and foundation movements in a semi-circular arch. In: COMPDYN Proceedings, pp. 2476–2491 (2023). https://www.scopus.com/inward/record.uri?eid=2-s2.0-85175847244&partnerID=40&md5=8edeef8ffd0b5e72961ce432ffed7a61
32. Iannuzzo, A., Mallardo, V.: A novel approach to model differential settlements and crack patterns in masonry structures. Eng. Struct. **323**, 119220 (2025). https://doi.org/10.1016/j.engstruct.2024.119220
33. Iannuzzo, A., Mele, T.V., Block, P.: Stability and load-bearing capacity assessment of a deformed multi-span masonry bridge using the PRD method. Int. J. Masonry Res. Innov. **6**(4), 422–445 (2021). https://doi.org/10.1504/IJMRI.2021.118842
34. Iannuzzo, A., Montanino, A.: A limit analysis-based CASS approach for the in-plane seismic capacity of masonry façades. Int. J. Solids Struct. **289**, 112633 (2024). https://doi.org/10.1016/j.ijsolstr.2023.112633
35. Itasca Consulting Group: 3DEC — Three-Dimensional Distinct Element Code, Version 7.0. Itasca Consulting Group, Minneapolis, Minnesota (2020). https://www.itascacg.com/software/3dec
36. Lemos, J.V.: Assessment of the ultimate load of a masonry arch using discrete elements. Computer Methods in Structural Masonry **3**, 294–302 (1995). no open-access link available
37. Lemos, J.V.: Discrete element modeling of masonry structures. Int. J. Architectural Heritage **1**(2), 190–213 (2007). https://doi.org/10.1080/15583050601176868
38. Lourenço, P.B.: Computations on historic masonry structures. Prog. Struct. Mat. Eng. **4**(3), 301–319 (2002). https://doi.org/10.1002/pse.120
39. McInerney, J., DeJong, M.J.: Discrete element modelling of groin vault displacement capacity. Int. J. Architectural Heritage **9**(8), 1037–1049 (2015). https://doi.org/10.1080/15583058.2014.923953
40. Montanino, A., Iannuzzo, A.: A quadrilateral plate-type finite element to model stress singularities in no-tension materials. Comput. Methods Appl. Mech. Eng. **432**, 117433 (2024). https://doi.org/10.1016/j.cma.2024.117433
41. Montanino, A., Olivieri, C., Zuccaro, G., Angelillo, M.: From stress to shape: Equilibrium of cloister and cross vaults. Appl. Sci. **11**(9), 3846 (2021). https://doi.org/10.3390/app11093846

42. Mousavian, E., Kibriya, G., Bagi, K., Iannuzzo, A.: Multi-surface plasticity model for analysis of complex interlocking assemblies. In: Structures and Architecture, pp. 893–900. CRC Press (2025)
43. Nodargi, N.A., Bisegna, P.: Thrust line analysis revisited and applied to optimization of masonry arches. Int. J. Mech. Sci. **179**, 105690 (2020). https://doi.org/10.1016/j.ijmecsci.2020.105690
44. Nodargi, N.A., Bisegna, P.: A unifying computational approach for the lower-bound limit analysis of systems of masonry arches and buttresses. Eng. Struct. **221**, 110999 (2020). https://doi.org/10.1016/j.engstruct.2020.110999
45. Ochsendorf, J.A.: The masonry arch on spreading supports. Struct. Eng. **84**(2), 29–35 (2006). https://www.istructe.org/journal/volumes/volume-84-(2006)/issue-2/the-masonry-arch-on-spreading-supports/
46. Ochsendorf, J.A.: Collapse of masonry structures (2002). Ph.D. thesis
47. Olivieri, C.: FORMERLY-Math: Constrained form-finding through membrane equilibrium analysis in Mathematica. Softw. Impacts **16**, 100512 (2023). https://doi.org/10.1016/j.simpa.2023.100512
48. Olivieri, C., Cocking, S., Fabbrocino, F., Iannuzzo, A., Placidi, L., Adriaenssens, S.: Seismic capacity of purely compressed shells based on airy stress function. Continuum Mech. Thermodyn. **37**(2), 21 (2025). https://doi.org/10.1007/s00161-024-01350-z
49. Olivieri, C., Fortunato, A., DeJong, M.: A new membrane equilibrium solution for masonry railway bridges: the case study of Marsh Lane Bridge. Int. J. Masonry Res. Innov. **6**(4), 446–471 (2021). https://doi.org/10.1504/IJMRI.2021.118831
50. Pagnoni, T., Vanzi, I.: Experimental and numerical study of the seismic response of block structures (1995). no open-access link available
51. Papantonopoulos, C., Psycharis, I., Papastamatiou, D., Lemos, J., Mouzakis, H.: Numerical prediction of the earthquake response of classical columns using the distinct element method. Earthquake Eng. Struct. Dyn. **31**(9), 1699–1717 (2002). https://doi.org/10.1002/eqe.185
52. Papastamatiou, D., Psycharis, I.: Seismic response of unbraced multidrum columns. Earthquake Eng. Struct. Dyn. **22**(10), 857–872 (1993). https://doi.org/10.1002/eqe.4290221004
53. Paris, V., Gobbin, F., Nannei, V., Resmini, M., Mirabella Roberti, G.: Distinct element method analyses for damage assessment: The northern spur of valverde bulwark in the venetian fortress of bergamo. Int. J. Archit. Heritage **19**(5), 687–701 (2025). https://doi.org/10.1080/15583058.2024.2345701. cited by: 3
54. Paris, V., Olivieri, C., Adriaenssens, S.: The impact of construction on the structural design of a complex masonry curved shell. Int. J. Space Struct. **40**(2–3), 180–194 (2025). https://doi.org/10.1177/09560599251381901. cited by: 3; All Open Access, Hybrid Gold Open Access
55. Pingaro, N., Buzzetti, M., Milani, G.: Advanced FE nonlinear numerical modeling to predict historical masonry vaults failure: Assessment of risk collapse for a long span cloister vault heavily loaded at the crown by means of a general-purpose numerical protocol. Eng. Fail. Anal. **167**, 109070 (2025). https://doi.org/10.1016/j.engfailanal.2024.109070
56. Pingaro, N., Cardani, G., Coronelli, D., Milani, G.: On the stability of masonry arches through limit analysis and a nonlinear finite element-based method. In: International Conference on Protection of Historical Constructions, pp. 201–208. Springer (2025). https://doi.org/10.1007/978-3-031-87316-4_25

57. Pourfouladi, M., Pingaro, N., Valente, M.: Polibrick plugin as a parametric tool for digital stereotomy modelling. Comput. Struct. **311**, 107722 (2025). https://doi.org/10.1016/j.compstruc.2025.107722
58. Ranaudo, F., Van Mele, T., Block, P.: A low-carbon, funicular concrete floor system: Design and engineering of the HiLo floors. Tech. rep., ETH Zurich, Block Research Group (2021). https://doi.org/10.2749/ghent.2021.2016, https://www.research-collection.ethz.ch/handle/20.500.11850/479967
59. Rippmann, M., Liew, A., Van Mele, T., Block, P.: Design, fabrication and testing of discrete 3D sand-printed floor prototypes. Mater. Today Commun. **15**, 254–259 (2018). https://doi.org/10.1016/j.mtcomm.2018.08.002
60. Robert McNeel & Associates: Rhinoceros 3D. Robert McNeel & Associates, Seattle, WA (2023). https://www.rhino3d.com
61. Roberti, G.M., Ruscica, G., Paris, V.: From the herringbone dome by sangallo to the serlio floor of emy (and beyond). Curved Layered Struct. **8**(1), 259–270 (2021). https://doi.org/10.1515/cls-2021-0023. cited by: 3; All Open Access, Gold Open Access, Green Open Access
62. Sánchez Robles, C.: Mass piedra — coordinadora. https://masspiedra.org/ (2025). Accessed 2025
63. Shi, G.H.: Discontinuous Deformation Analysis: A New Numerical Model for the Statics and Dynamics of Deformable Block Structures. Ph.D. thesis, University of California, Berkeley (1992). https://escholarship.org/uc/item/3027n5vk